Cell Reports
Physical Science

CellPress
OPEN ACCESS

Article

Catalytic decomposition of NO_2 over a copper-decorated metal–organic framework by non-thermal plasma

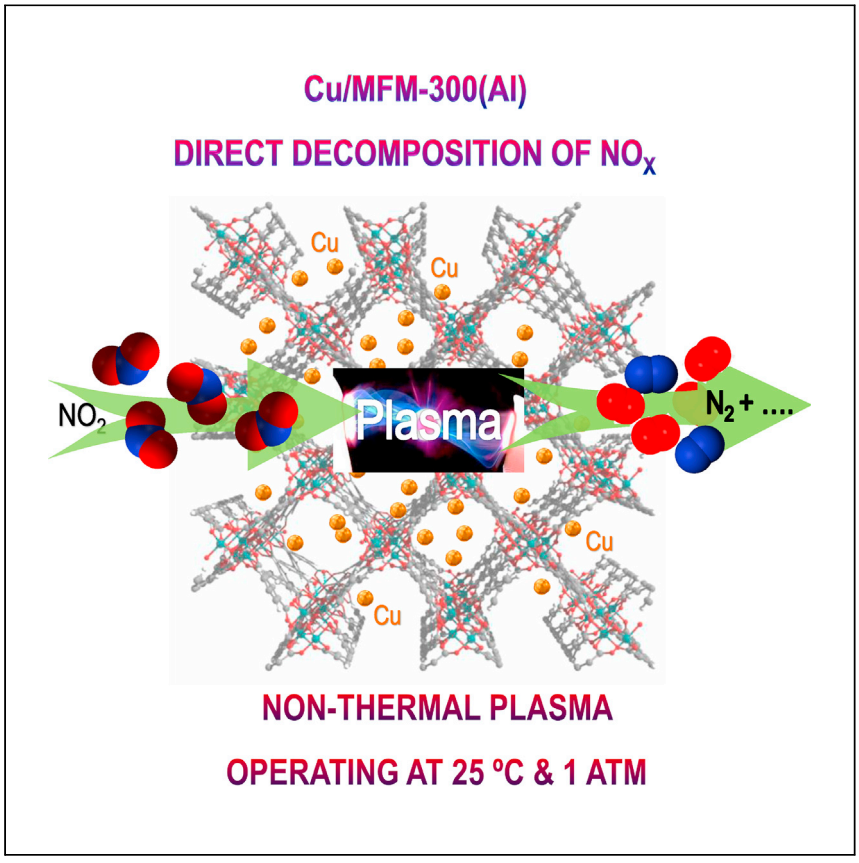

Nitrogen oxide causes significant effects on the environment and human health. Xu et al. report, to the best of their knowledge, the first example of nonthermal plasma-activated direct decomposition of NO_2 over stable and efficient metal-organic framework-based catalysts at room temperature and without the use of NH_3 or other reducing agents.

Shaojun Xu, Xue Han, Yujie Ma, ..., Christopher Hardacre, Sihai Yang, Martin Schröder

sihai.yang@manchester.ac.uk (S.Y.)
m.schroder@manchester.ac.uk (M.S.)

HIGHLIGHTS

MOF-based catalyst with plasma-activation to directly convert NO_2

Cu/MFM-300(Al) shows a high NO_2 conversion, N_2 selectivity, and long-term stability

$Cu^{2+}\cdots NO$ nitrosylic adducts formed facilitate NO dissociation and N_2 selectivity

Xu et al., Cell Reports Physical Science 2, 100349
February 24, 2021
https://doi.org/10.1016/j.xcrp.2021.100349

Cell Reports
Physical Science

CellPress
OPEN ACCESS

Article

Catalytic decomposition of NO_2 over a copper-decorated metal–organic framework by non-thermal plasma

Shaojun Xu,[1,2] Xue Han,[1] Yujie Ma,[1] Thien D. Duong,[1] Longfei Lin,[1] Emma K. Gibson,[2,3] Alena Sheveleva,[1] Sarayute Chansai,[4] Alex Walton,[1,5] Duc-The Ngo,[6] Mark D. Frogley,[7] Chiu C. Tang,[7] Floriana Tuna,[1] Eric J.L. McInnes,[1] C. Richard A. Catlow,[2,8,9] Christopher Hardacre,[4] Sihai Yang,[1,*] and Martin Schröder[1,10,*]

SUMMARY

Efficient catalytic conversion of NO_2 to non-harmful species remains an important target for research. State-of-the-art $deNO_x$ processes are based upon ammonia (NH_3)-assisted selective catalytic reduction (NH_3-SCR) over Cu-exchanged zeolites at elevated temperatures. Here, we describe a highly efficient non-thermal plasma (NTP) $deNO_x$ process catalyzed by a Cu-embedded metal-organic framework, Cu/MFM-300(Al), at room temperature. Under NTP activation at 25°C, Cu/MFM-300(Al) enables direct decomposition of NO_2 into N_2, NO, N_2O, and O_2 without the use of NH_3 or other reducing agents. NO_2 conversion of 96% with a N_2 selectivity of 82% at a turnover frequency of 2.9 h^{-1} is achieved, comparable to leading NH_3-SCR catalysts that use NH_3 operating at 250°C–550°C. The mechanism for the rate-determining step ($NO \rightarrow N_2$) is elucidated by *in operando* diffuse reflectance infrared Fourier transform spectroscopy, and electron paramagnetic resonance spectroscopy confirms the formation of $Cu^{2+}\cdots NO$ nitrosylic adducts on Cu/MFM-300(Al), which facilitates NO dissociation and results in the notable N_2 selectivity.

INTRODUCTION

Nitrogen oxide (NO_x) is the cause of significant effects on the environment and human health.[1–3] Nitrogen dioxide (NO_2) is the most toxic and prevalent form of NO_x in the atmosphere, and its removal and catalytic degradation into non-harmful species (i.e., N_2) are important challenges. A great deal of effort has been devoted to developing catalysts for $deNO_x$ processes, with a focus on NO reduction from exhaust gases. The NH_3-assisted selective catalytic reduction (NH_3-SCR) over Cu-exchanged zeolites is by far the most effective method to reduce NO_x to N_2 and H_2O[4,5] (Equations 1, 2, and 3). However, this process has several inherent limitations, notably the high operating temperature (typically 250°C–550°C), high running cost of reductants, use of corrosive and toxic NH_3, and the potential release of NH_3 into the atmosphere.[1,2] In contrast, the catalytic degradation of NO_2 for domestic environments is poorly studied. The development of new efficient catalysts and catalytic processes to enable the direct decomposition of NO_2 at room temperature and without the use of reducing agents (Equation 4) has, therefore, attracted considerable attention.[6–10]

[1]Department of Chemistry, University of Manchester, Manchester M13 9PL, UK

[2]UK Catalysis Hub, Research Complex at Harwell, Rutherford Appleton Laboratory, Harwell, OX11 0FA, UK

[3]School of Chemistry, Joseph Black Building, University of Glasgow, Glasgow G12 8QQ, UK

[4]Department of Chemical Engineering and Analytical Science, University of Manchester, Manchester M13 9PL, UK

[5]Photon Science Institute, University of Manchester, Manchester M13 9PL, UK

[6]Department of Materials, University of Manchester, Manchester M13 9PL, UK

[7]Diamond Light Source, Harwell Science Campus, Oxfordshire OX11 0DE, UK

[8]School of Chemistry, Cardiff University, Main Building, Park Place, Cardiff CF10 3AT, UK

[9]Department of Chemistry, University College London, 20 Gordon Street, London WC1H 0AJ, UK

[10]Lead contact

*Correspondence: sihai.yang@manchester.ac.uk (S.Y.), m.schroder@manchester.ac.uk (M.S.)

https://doi.org/10.1016/j.xcrp.2021.100349

$$4NH_3 + 4NO + O_2 \rightarrow 4N_2 + 6H_2O \quad \text{(Equation 1)}$$

$$6NO_2 + 8NH_3 \rightarrow 7N_2 + 12H_2O \quad \text{(Equation 2)}$$

$$NO + NO_2NH_3 \rightarrow 2N_2 + 3H_2O \quad \text{(Equation 3)}$$

$$2NO_2 \rightarrow N_2 + 2O_2 \quad \text{(Equation 4)}$$

Porous metal-organic framework (MOF) materials show promise for the highly selective adsorption and separation of NO_2 at room temperature under both dry and humid conditions.[1,9,11–16] However, the stability and reusability of MOFs for NO_2 adsorption has only been demonstrated in exceptional cases.[9,11] Due to their high porosity and tailored-to-design pore functionality, MOFs can also be used as heterogeneous catalysts and catalyst supports.[17,18] For example, embedding metal nanoparticles (MNPs) into MOF pores can overcome the aggregation of MNP and thus improve the catalytic stability.[17,19,20] Moreover, the synergistic effects between the pore interior of MOFs and MNPs can result in highly desirable product selectivities.[21] However, the application of MOF-based catalysts in deNO_x processes has been rarely explored,[22–24] primarily due to the limited stability of MOFs against highly corrosive NO_2 and NH_3 at elevated temperatures.

Non-thermal plasma (NTP) activation can promote deNO_x processes at room temperature by generating highly reactive species, especially vibrationally and electronically excited states of molecules (e.g., N_2, O_2, NO), N and O atoms, radicals, and electrons with a typical electron temperature of 10^4°C.[8,10,25,26] NTP-promoted deNO_x processes can be readily tuned by balancing the power input, and potentially this enhances the overall energy efficiency by controlling the reaction pathway within a reversible and active heterogeneous catalyst. Recently, NTP activation in MOF-based catalysts has been shown to enhance performance in water-gas shift reactions, with the structure and porosity of the MOF being preserved.[18] NTP-modified [Cu_3(BTC)] (H_3BTC = benzene-1,3,5-tricarboxylic acid) has been shown to give high catalytic conversion of NO (~98%) owing to the abundant Cu sites generated from the decomposition of the framework.[10] However, the efficient catalytic conversion of NO_2 into N_2 over MOFs remains a highly challenging and important research pipeline.

Here, we report, to the best of our knowledge, the first example of NTP-activated direct decomposition of NO_2 over MOF-based catalysts at room temperature and without the use of NH_3 or other reducing agents. At 25°C and 1.0 bar, 7 wt% Cu-embedded MFM-300(Al) enables a near-quantitative conversion of NO_2 (500 ppm diluted in He) into N_2, NO, and N_2O with selectivities of 82%, 11%, and 7%, respectively. Cu/MFM-300(Al) also shows excellent catalytic stability and an exceptional turnover frequency (TOF) value of 2.9 h^{-1}. It should be emphasized that theoretical TOF values are quoted in this study, and the determination of the effective TOF is described in Tables S4 and S5. *In operando* diffuse reflectance infrared Fourier transform spectroscopy (DRIFTS) has been applied to study the adsorption and reactivity of NO_2 on Cu/MFM-300(Al) and reveals strong adsorption of the key reaction intermediate NO on the Cu sites, thus promoting its efficient conversion to N_2. Electron paramagnetic resonance (EPR) spectroscopy confirms the formation of a triplet spin state that is consistent with ferromagnetic interaction between Cu^{2+} and NO.

RESULTS

Synthesis and characterization of MOF-based catalysts

MFM-300(Al) has been selected in this study due to its ultra-high structural stability and reversible adsorption of NO_2 (14.1 mmol g^{-1} at 298 K and 1.0 bar).[9] MFM-300(Al) has an

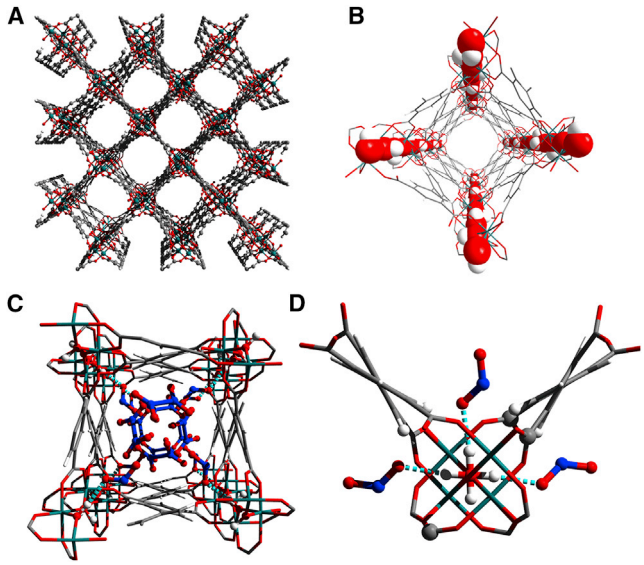

Figure 1. Views of crystal structure of MFM-300(Al) and its adsorption sites for NO_2

(A) View of the 3-dimensional (3D) framework structure of MFM-300(Al).

(B) View of the square-shaped channel comprising the corner-sharing extended octahedral chain of $[AlO_4(OH)_2]_\infty$. The μ_2-(OH) groups are highlighted as a space-filling model and linked to each other in a *cis*-configuration (Al, green; C, gray; O_2, red; H_2, white; N_2: blue).

(C and D) Views of binding sites for adsorbed NO_2 molecules within MFM-300(Al).[9]

open framework with 1-dimensional channels (~6 × 6 $Å^2$) constructed by $[AlO_4(OH)_2]_\infty$ chains bridged by organic linkers (Figures 1A and 1B).[27] The *cis*-configured hydroxyl groups protrude into the square-shaped channels, affording accessible μ_2-OH sites to bind guest species, notably with NO_2 (Figures 1C and 1D). The activity of the MOF as a catalyst support has been evaluated by comparing to the benchmark γ-Al_2O_3 (with mesopores of 25 Å) and ZSM-5 (with a pore size of 6 Å). Both CuO and Cu NPs have been investigated as active sites for the NTP-activated deNO_x reaction to reveal the impact of the oxidation state of Cu on reactivity.

Catalysts based upon CuO/support (support = MFM-300(Al), γ-Al_2O_3, and ZSM-5) were prepared using an incipient wetness impregnation method (see Supplemental experimental methods) followed by calcination at 250°C in air for 12 h. The corresponding Cu-embedded catalysts were prepared by reducing the CuO-embedded catalysts under a flow of 5% H_2 at 250°C for 12 h. High-resolution synchrotron X-ray powder diffraction confirmed the retention of the crystal structures of all of the catalysts on the loading of CuO and Cu (Figures 2A and 2B), and the loading of MNPs was determined by elemental analysis (Table S1). Transmission electron microscopy (TEM) confirms that there are no changes in the sample morphology on the loading of CuO and Cu (uniform particle size of ~1 nm, Figures 2C and 2D), and energy-dispersive X-ray spectroscopy (EDX) mapping shows a homogeneous distribution of the loaded Cu sites (Figure S3). Synchrotron Fourier transform infrared spectroscopy (FTIR) spectra of MFM-300(Al) show a reduction in the intensity of the μ_2-OH stretching band at 3,687 cm^{-1}, coupled with peak broadening and a slight redshift on the loading of CuO and Cu, indicating interactions between the μ_2-OH groups and Cu/CuO NPs (Figure S4).[20,28–30] N_2 adsorption isotherms at 77 K confirmed that loading of Cu/CuO NPs leads to small reductions in the porosity of all of the catalysts and that the NTP treatment has a negligible impact on the porosity of these materials (Table S2).

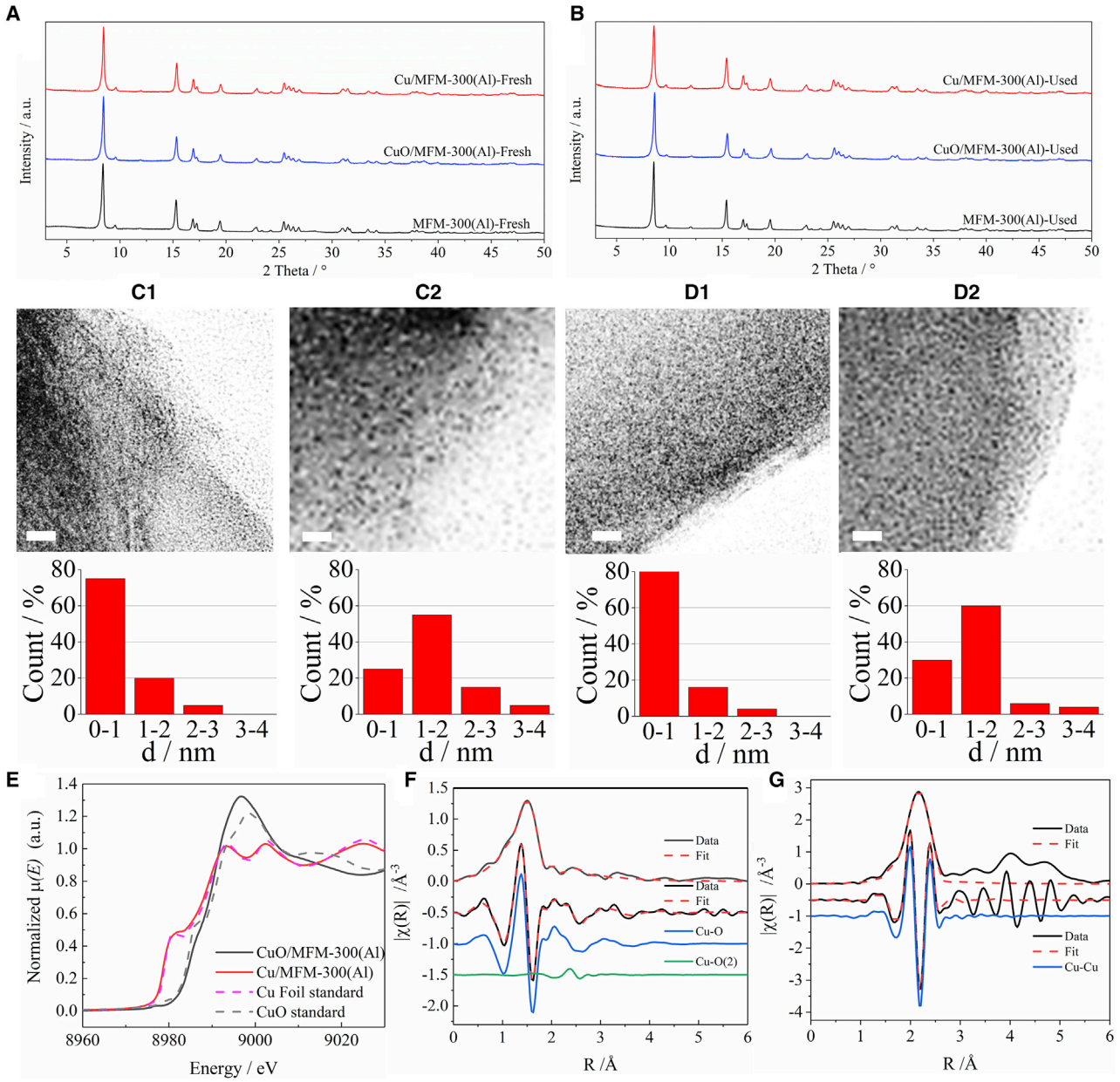

Figure 2. Characterization of catalysts

(A–D) High-resolution synchrotron X-ray powder diffraction of MFM-300(Al), CuO/MFM-300(Al) and Cu/MFM-300(Al) (A) before (fresh) and (B) after (used) NTP-assisted NO_2 decomposition. TEM micrograph of Cu/MFM-300(Al) (C1) before and (C2) after, and of CuO/MFM-300(Al) (D1) before and (D2) after deNO_2 reaction (scale bars 5 nm). The corresponding particle size distribution graphs are shown underneath the TEM views.

(E) Normalized Cu K-edge XANES spectra of fresh Cu/MFM-300(Al) and CuO/MFM-300(Al) recorded after drying in He at 250°C and standard XANES spectra of a Cu foil and CuO recorded as references.

(F and G) Stacked plots of the magnitude (top) and imaginary (bottom) non-phase corrected Fourier-transformed Cu K-edge EXAFS of (F) CuO/MFM-300(Al) and of (G) Cu/MFM-300(Al) recorded after drying in He at 250°C. These have been plotted with the fit constructed from Cu-O and Cu-Cu scattering paths.

Continuous-wave EPR spectra of desolvated samples of Cu- and CuO-embedded MFM-300(Al) (Figures S5 and S6, Table S6) reveal 2 types of Cu^{2+} sites in both cases: (1) one that is characteristic of a monomeric Cu(II) with a tetragonal coordination environment, manifested in an axial EPR signal with $g_z >> g_{x,y} > 2$ and a

well-resolved 4-line pattern in the z component due to highly axial hyperfine interactions with the $I = 3/2$ $^{63/65}$Cu; and (2) one that is characterized by a broad isotropic signal and is typical of small NPs or clusters in which Cu(II) is involved in spin-spin interactions with its neighbors. Larger NPs are usually EPR inactive due to extensive spin-spin interactions that stabilize a non-magnetic spin state.[28] Similarly, Cu^{+} ($3d^{10}$) is EPR inactive.

To identify further the electronic properties and local coordination environment of the embedded Cu species, we performed the *ex situ* X-ray absorption fine structure (XAFS) spectroscopy of CuO/MFM-300(Al) and Cu/MFM-300(Al) at the Cu K-edge. In the near-edge region (Figure 2E), the X-ray absorption near-edge structure (XANES) spectra of Cu/MFM-300(Al) compares well with the Cu foil reference, and the CuO/MFM-300(Al) appears to be similar to CuO. The Fourier transform of the k^2 weighted extended XAFS (EXAFS) data for CuO/MFM-300(Al) compared to that of a CuO reference material shows (Figure S7, Table S7) much lower intensity of the features at a longer distance, suggesting that these CuO clusters in the MOF are small. A reasonable fit of the data (Figure 2F) was obtained using 2 Cu-O scattering paths at 1.936 $\pm$ 0.003 and 2.9 $\pm$ 0.2 Å, the distances being consistent with CuO. From the reduced intensity of the μ_2-OH stretching band at 3,687 cm^{-1} observed in the synchrotron FTIR spectra (Figure S4), the Cu site is likely attached to the framework O_2 centers of MFM-300(Al). Fitting the EXAFS spectra of Cu/MFM-300(Al) using the 1st shell Cu-Cu scattering path provides a good fit to Cu metal (Figure 2G). The coordination number of the 1st shell Cu-Cu path is 11 $\pm$ 1, with a calculated Cu particle size of 3.5 $\pm$ 0.5 nm,[29] which is consistent with the transmission electron microscopy (TEM) measurements of the Cu particle size. Thus, reduction of CuO/MFM-300(Al) with H_2 generates Cu/MFM-300(Al), in which the Cu^{2+} ions are reduced and slightly sintered to give Cu^0 with an average particle size of 3 nm.

Catalytic reactions

A typical vehicle emission contains 100–1,000 ppm NO_x (mainly NO and NO_2) and 5% O_2 in N_2.[1,2] To examine the performance of these catalysts for the direct decomposition of NO_2, a model gas stream of 500 ppm NO_2 diluted in He was used as the feed for catalysis tests throughout the present study. In the absence of plasma and catalyst, the empty reactor showed negligible conversion of NO_2 at 25°C–250°C, while the presence of catalysts alone without the plasma at 25°C gives very low conversion of NO_2 (<10%). In contrast, in the absence of a catalyst at 25°C, gas phase NTP gives a NO_2 conversion of 66%, but a low N_2 selectivity of 13% and a high NO selectivity of 81%. These results suggest that NO_2 can be readily dissociated to NO by gas phase NTP, but further reduction of NO to N_2 (the rate-determining step) cannot be achieved by NTP alone, which is consistent with previous reports on the NTP-assisted decomposition of NO_x in which only a small amount of N_2 can be produced via the collision of NO_x with the excited state of He* in gas phase.[25,30]

The catalytic activity and product selectivities for NO_2 decomposition have been systematically investigated for all 9 catalysts (namely, bare support, CuO/support and Cu/support; support = MFM-300(Al), γ-Al_2O_3, and ZSM-5) under steady-state plasma conditions: the specific energy input (SEI) was ~0.4 kJ L^{-1} at a frequency of 10 kHz and alternating current (AC) peak-to-peak voltage ($V_{pk\text{-}pk}$), of 13 $\pm$ 0.5 kV at 25°C (Figure 3; Table S3). The bare supports of γ-Al_2O_3, ZSM-5, and MFM-300(Al) show enhanced NO_2 conversions (71%, 76%, and 92%, respectively) and N_2 selectivities (15%, 35%, and 46%, respectively), compared with the tests under thermal

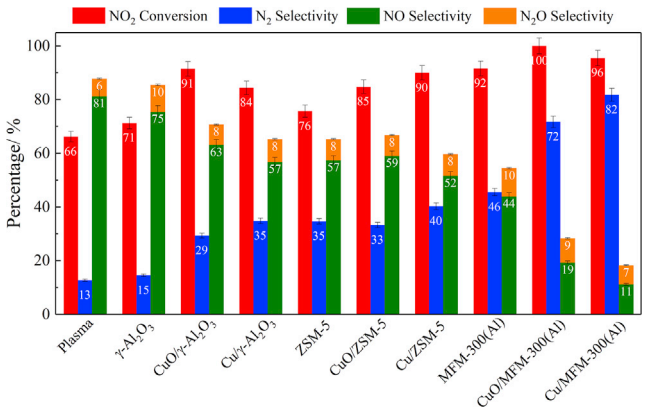

Figure 3. Comparison of results for all of the catalysts in this study

NO_2 conversion and product selectivities over catalysts supported by γ-Al_2O_3, ZSM-5, and MFM-300(Al) under steady-state NTP conditions (0.4 kJ L^{-1}, 13 ± 0.5 kV, 10 kHz, 25°C) using a feed of 500 ppm NO_2 in He. The control experiment without catalyst is labeled "Plasma." Each data point is an average of 3 consecutive measurements with an error of < ±3% for NO_2 conversion and < ±4% for product selectivity.

conditions (NO_2 conversions <10%). The NO_2 conversions are enhanced by the CuO- and Cu-embedded catalysts. A small improvement in the N_2 selectivity was observed for CuO- or Cu-embedded γ-Al_2O_3 and ZSM-5, with the highest selectivity of 40% achieved in Cu/ZSM-5. More significant increases in N_2 selectivity were achieved with the MFM-300(Al) supported catalysts, in which CuO/MFM-300(Al) showed N_2 selectivity of 72% with a quantitative conversion of NO_2, and Cu/MFM-300(Al) achieved the highest N_2 selectivity of 82% with NO_2 conversion >96% (equivalent to an energy efficiency of 0.06 mmol kJ^{-1} for the dissociation of NO_2). These observations indicate a synergistic positive effect on N_2 selectivities between the loaded Cu-NPs and the MOF host. More important, Cu/MFM-300(Al) also exhibits a high TOF value of 2.9 h^{-1} without the use of any reductant, thus outperforming the state-of-the-art Cu-based catalysts for the direct decomposition of NO_2 (Table S4). For example, the CuO/Al_2O_3 catalyst shows a TOF of 0.1 and 2.8 h^{-1} at 325°C and 520°C, respectively, with N_2 selectivities of ~50%.[6] Recently, a Cu-embedded ZSM-5 catalyst has been reported to show a TOF value of 1.8 h^{-1} and a N_2 selectivity of 86% for NTP-activated deNO_x reactions using H_2 as reducing agent at 25°C[31] (Table S5). It is worth noting that the superior catalytic activity of Cu/MFM-300(Al) is comparable to that of the leading NH_3-SCR catalysts based upon Cu-exchanged SSZ-13 zeolites, which critically rely on the use of NH_3 and operate at 250°C–550°C, with TOF values of 1.9–2.2 h^{-1} and N_2 selectivities of 85%–100%.[32]

Stability tests

It has been widely reported that MNP-embedded catalysts for deNO_x reactions often suffer from rapid deactivation and thus have poor time-on-stream (ToS) stabilities due to the oxidation of active metal sites.[5,33] We sought to investigate the ToS stability of all three Cu-embedded catalysts in this study. As expected, Cu/γ-Al_2O_3 and Cu/ZSM-5 catalysts show steady deactivation under reaction conditions (Figure 4A) due to the formation of aggregated CuO particles, which has been confirmed by powder X-ray diffraction (PXRD) (Figure S8). In comparison, Cu/MFM-300(Al) exhibits excellent catalytic stability, with a ToS of >200 min, and X-ray photoelectron spectroscopy (XPS) analysis confirms that in fresh Cu/MFM-300(Al) catalyst, 75% of the Cu(II) was reduced to Cu(I) and Cu(0), while 60% of the

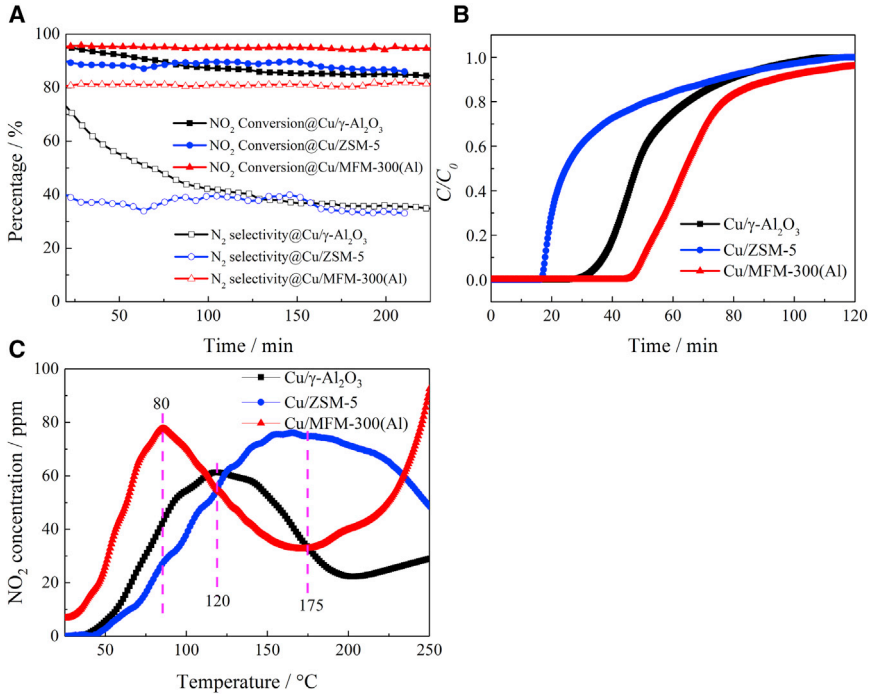

Figure 4. Comparison of the time-on-stream stability, breakthrough capacity, and NO_2-temperature-programmed desorption plots for various catalysts

(A) Comparison of the time-dependent ToS plots for NO_2 conversion and N_2 selectivity over various Cu-embedded catalysts under NTP conditions (0.4 kJ L^{-1}, 10 kHz, 25°C, 500 ppm NO_2 in He and atmospheric pressure).

(B) Dynamic breakthrough experiments for Cu/support catalyst (support = MFM-300(Al), ZSM-5, and γ-Al_2O_3) at 25°C using the same NO_2 gas feed as in catalysis tests.

(C) NO_2-TPD plots of NO_2-saturated Cu/support (support = MFM-300(Al), ZSM-5, and γ-Al_2O_3) catalysts.

Cu species remained in the form of Cu(I) and Cu(0) in used Cu/MFM-300(Al) catalyst (Figure S9). Furthermore, PXRD analysis suggests the full retention of the crystal structure of all MOF-based catalysts after the reaction, and Cu or CuO aggregates of >5 nm[19,34] are not observed (Figure 2B). High-resolution TEM studies further confirm the negligible aggregation of CuO and Cu NPs within the MOF-based catalysts after the reaction (Figures 2C, 2D, and S3), and this retention of particle size is likely to be the basis for the high catalytic stability of the MFM-300(Al)-based catalysts.

Cu/MFM-300(Al) exhibits good stability in terms of NTP-promoted catalytic activity and structural integrity in the presence of water vapor up to a ToS of 250 min (Figure S10). The conversion of NO_2 (95%) on Cu/MFM-300(Al) was not affected by water vapor, although the selectivity for N_2 decreases from 82% to 61%. These results confirm that Cu-embedded MFM-300(Al) shows high resistance to competitive adsorption and maintains its high activity in the presence of water vapor.

Catalyst-NO_2 surface chemistry

The decomposition of NO_2 to N_2 and O_2 over Cu-based catalysts has been reported as a zero-order reaction, with the adsorption being the rate-determining step.[6] To gain further insights into the preferential adsorption of NO_2 in these materials, dynamic breakthrough experiments at 25°C using the same NO_2 gas feed were

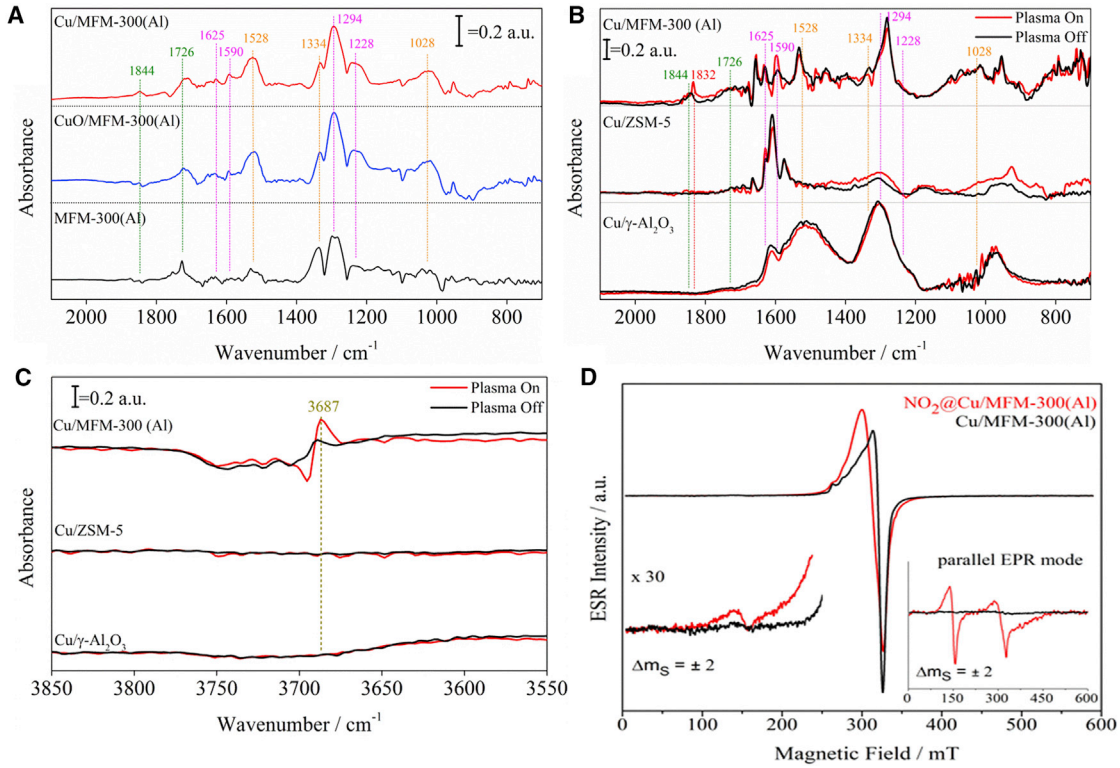

Figure 5. *In situ* and *in operando* DRIFTS spectra of Cu/MFM-300(Al), Cu/ZSM-5, and Cu/γ-Al_2O_3 as a function of NO_2 adsorption and reactions

(A) *In situ* DRIFTS spectra of adsorbed NO_2 on MFM-300(Al), CuO/MFM-300(Al), and Cu/MFM-300(Al). The background spectra for bare samples have been removed and gas phase NO_2 was removed using an Ar purge.

(B and C) *In operando* DRIFTS spectra over Cu/support catalysts (support = MFM-300(Al), ZSM-5, and γ-Al_2O_3) under steady-state NTP conditions (0.2 kJ L^{-1}, 7.5 ± 0.5 kV, 26 kHz, and 25°C with a NO_2 conversion of ~85%) using a feed of 500 ppm NO_2 in He. All DRIFTS spectra were recorded at a resolution of 4 cm^{-1}. The spectrum of bare samples has been subtracted.

(D) X-band (9.4 GHz) EPR spectra at 5 K of Cu/MFM-300(Al) before (black) and after (red) NO_2 loading. Inset: parallel-mode EPR spectra of the same samples revealing that the half-field forbidden transition ($\Delta m_S = \pm 2$) of the triplet state resulted from Cu-NO interaction.

conducted (Figures 4B and S11). These experiments confirmed that MFM-300(Al)-based materials showed notably higher retention of NO_2 than γ-Al_2O_3- and ZSM-5-based catalysts. Interestingly, embedding CuO and Cu NPs into all three types of supports had a positive impact on NO_2 adsorption, and Cu/MFM-300(Al) showed the strongest retention of NO_2 among all of the studied catalysts. Temperature-programmed desorption (TPD) plots confirm that Cu/MFM-300(Al) released significantly higher amounts of NO_2 than γ-Al_2O_3- and ZSM-5-based catalysts (Figures 4C and S12).

In situ DRIFTS has been used to investigate the adsorption of NO_2 (500 ppm diluted in He) on these catalysts at 25°C (Figures 5A and S13A). The differences in DRIFTS spectra (with the background of bare catalysts and the gas phase NO_2 removed) suggest the formation of various adsorbed nitro/nitrate species on the catalyst surface. In particular, the bands for monodentate and bidentate surface nitro/nitrate species at 1,590–1,500 cm^{-1}, 1,380–1,330 cm^{-1}, and 1,060–980 cm^{-1} and of bridging nitrates at 1,650–1,600 cm^{-1} and 1,290–1,210 cm^{-1} are observed for all of the catalysts studied, which is entirely consistent with previous reports.[35–40] Interestingly, NO_2-adsorbed Cu/MFM-300(Al) shows new bands at 1,844 and 1,726 cm^{-1}, which can be assigned to the formation of $M^+\cdots NO$ nitrosylic species[37,39]; these bands are not observed or are much weaker for γ-Al_2O_3- and ZSM-5-based catalysts

(Figure S13A). This is further confirmed by the DRIFTS spectra using NO as a probe, with peaks at 1,844 cm and 1,726 cm^{-1} observed on Cu/MFM-300(Al), but not on MFM-300(Al). This observation indicates that Cu/MFM-300(Al) can form unique $Cu^{2+}\cdots NO$ nitrosylic adducts with NO, thus greatly facilitating its further reduction to N_2 and leading to the observed excellent selectivity for N_2 formation. These results are consistent with the recent reports that MOFs provide an excellent platform to optimize both reaction conversion and product selectivity.[41,42]

X-band EPR spectroscopy of NO_2-loaded Cu/MFM-300(Al) reveals magnetic coupling between NO and Cu^{2+} (Figures 5D and S14, Table S8). Thus, the EPR spectrum of the NO_2-loaded sample displays a half-field transition at ~175 mT, characteristic of species with $S \geq 1$, which is non-observable for bare Cu/MFM-300(Al) and which confirms magneto dipole-dipole interaction between NO_x (S = 1/2) and Cu^{2+}(S = 1/2).[43] The spectrum for NO_2-loaded Cu/MFM-300(Al) differs dramatically from that of Cu/MFM-300(Al) in the field range with *g*-factor values close to 2. A similar spectrum was reported previously for adducts of NO molecule and copper sites.[44,45] Our tentative simulations support the formation of $Cu^{2+}\cdots NO$ adducts rather than $Cu^{2+}\cdots NO_2$ adducts (Figure S15).

Operando DRIFTS studies on the reaction pathway

The underlying catalyst-substrate interaction has been studied further by *in operando* DRIFTS experiments as a function of plasma on-off over the catalyst and reaction time (Figures 5B, 5C, and S13B). Upon ignition of plasma (0.2 kJ L^{-1}, 7.5 $\pm$ 0.5 kV, 26 kHz, and 25°C with a NO_2 conversion of ~85%), the bands of adsorbed nitro/nitrate species reduced rapidly on all of the catalysts, indicating the rapid conversion of these species. The bands at 1,844 cm and 1,726 cm^{-1} observed on NO_2-adsorbed Cu/MFM-300(Al) also reduced in intensity, indicating the rapid decomposition of $M^{+}\cdots NO$ nitrosylic complexes and the promoted reduction of NO to N_2. Interestingly, a new peak at 1,832 cm^{-1} (assigned to gas phase NO) appears upon switching the plasma on and disappears upon switching the plasma off, owing to the gas phase NO_2 dissociation under NTP conditions. More intriguing, a notable change in intensity has been observed for the μ_2-OH stretching mode at 3,687 cm^{-1} in Cu/MFM-300(Al) as a function of plasma on and off (Figure 5C), indicating the retrieval of accessible μ_2-OH sites from those occupied by NO_x species during the conversion of NO_2. Thus, the catalytic mechanism of NO_2 decomposition over Cu/MFM-300(Al) can be tentatively proposed as a three-step process: (1) NO_2 is reduced directly to NO and a small amount of N_2O in the gas phase by NTP, as confirmed by control experiments; (2) strong adsorption of NO_2 and intermediates to form surface nitro/nitrate/nitrite species on Cu/MFM-300(Al); (3) NTP-assisted surface decomposition of adsorbed NO_x species: the surface nitro/nitrate/nitrite species dissociate under high-energy electrons generated by NTP to yield N_2 and O_2, thus regenerating accessible active sites at the surface. The excellent catalytic performance of Cu/MFM-300(Al) originates from a combination of optimal pore size, synergistic effects between the MOF interior and the embedded Cu NPs, high materials stability, and strong adsorption of NO_2.

DISCUSSION

There are powerful drivers for the development of efficient deNO_x systems that can operate at room temperature and avoid the use of toxic reductants. A new process combining robust MOF-based catalysts and NTP activation has been developed for one-through conversion of NO_2 into N_2 without using any external reducing agent at room temperature. The rigid and robust open structure of MFM-300(Al) offers an

excellent platform to embed uniformly dispersed Cu NPs of diameters of ~1 nm using a simple incipient wetness impregnation method. Cu/MFM-300(Al) shows simultaneously high NO_2 conversion and high N_2 selectivity, as well as excellent long-term stability under the NTP activation at 25°C and 1.0 bar. The high catalytic activity of Cu/MFM-300(Al) is attributed to the unique formation of $Cu^{2+}\cdots NO$ nitrosylic adducts, which facilitates the dissociation of NO to improve the yield of N_2. Compared with conventional thermal-based catalysis, NTP activation can effectively preserve the structure and porosity of MOF-based catalysts. Coupled with emerging stable MOFs showing ultra-high and selective NO_2 adsorption, we now seek to design new MOF-based catalysts to drive the future development of efficient reductant-free deNO_x processes to mitigate air pollutants.

EXPERIMENTAL PROCEDURES

Resource availability

Lead contact

Further information and requests for resources and reagents should be directed to and will be fulfilled by the lead contact, Prof. Martin Schröder (m.schroder@manchester.ac.uk).

Materials availability

This study did not generate new unique materials.

Data and code availability

All of the data associated with the study are included in the article and the supplemental experimental procedures. Additional information is available from the lead contact upon reasonable request.

Catalyst preparation

All of the chemicals were obtained from Sigma-Aldrich and used as received. The catalysts were prepared using supports of γ-Al_2O_3, ZSM-5, and MFM-300(Al). γ-Al_2O_3 and ZSM-5 were purchased from Sigma-Aldrich and used as received. MFM-300(Al) was synthesized following our previously reported method.[27] The loading of Cu (7 wt%) to the catalyst supports was carried out using the incipient wetness impregnation method. As illustrated in Figure S1, in a typical experiment, a known amount of $Cu(NO_3)_2\cdot 3H_2O$ was dissolved in 2 mL deionized water. The solution was then added to 100 mg γ-Al_2O_3, ZSM-5, or MFM-300(Al) and a slurry formed in each case, which was dried in an oven at 80°C for 1 h. The dried sample of $Cu(NO_3)_2$/support was then oxidized at 250°C (heating ramp: 5°C min^{-1}) for 12 h in air to produce the corresponding CuO/support as catalysts. To prepare the Cu/support catalysts, the CuO/support sample was reduced at 250°C under a 5% H_2 flow (balanced in Ar, 70 mL min^{-1}, heating ramp: 5°C min^{-1}) for 12 h.

Catalyst testing

The catalytic activity and selectivity of NO_2 decomposition over these catalysts have been carried out under both conventional thermal heating and NTP activation conditions (Figure S2). The gas feed contained 500 ppm NO_2 diluted in a flow He. The total flow of 100 mL min^{-1} at 25°C was controlled by mass flow controllers (MKS Instruments), and the same gas feed was used throughout for catalysis tests in this study. Before the reaction, all of the catalysts were pre-treated with a dry flow of He for 1 h at 80°C to remove moisture. The NO_2/He gas mixture was then passed through a fixed-bed reactor and the catalytic performance of each catalyst tested.

For thermal activation, a reactor of 6 mm outer diameter (OD) quartz tube was used and the catalyst held in place between quartz wool plugs. The reactor was placed in a tube

furnace and the reaction conducted from 25°C to 250°C. For NTP activation, a reactor comprising 2 coaxial quartz tubes of 6 mm OD for the outer tube and a 3-mm OD inner tube were used to give a discharge gap of 0.5 mm. The outer tube was covered by a metal mesh electrode, and a metal wire electrode was placed inside the inner tube. The outer electrode was connected to a high-voltage output and the inner electrode grounded. The catalyst was packed in the discharge region to ensure that the plasma was generated only around the catalyst. The plasma was ignited by an alternating current power source (CPT-2000K, 0–25 kV, 10 kHz). The AC peak-to-peak voltage (*V*) was measured using a high-voltage probe, and the voltage across an internal capacitor (0.47 μF) placed between an electrode and ground was measured to obtain the charge (*Q*) generated by the discharge. The electrical parameters were recorded in real-time online using an oscilloscope (Tektronix TDS 2022B), and the discharge power was calculated using the area of the Q-V Lissajous figure, as detailed in our previous work.[46,47] The discharge power was ~0.6 ± 0.05 W and the SEI was ~0.4 kJ L^{-1} at a frequency of 10 kHz and AC peak-to-peak voltage ($V_{pk\text{-}pk}$) ~13 ± 0.5 kV. The temperature was controlled by a fan and monitored by an infrared thermometer (IRT670, General Tools & Instruments).

To test the water stability of the catalysts, the Cu/MFM-300(Al) catalyst with MFM-300(Al) as a benchmark were tested in the plasma reaction in the presence of water vapor. Water and NO_2 were introduced to the reactor separately to avoid the pre-reaction of NO_2 and H_2O in the pipeline. The catalysts were treated with 2.8% H_2O vapor in He at 25°C with a flow rate of 100 mL min^{-1} for 250 min. The activity of the catalyst was then tested in plasma for 250 min under the same operating conditions as above in the absence of water.

Analysis of gaseous products emitted from the reactor was carried out using (1) a Bruker Matrix MG5 FTIR spectrometer (resolution = 0.5 cm^{-1}) for NO_x (NO_2, NO, and N_2O) and (2) a mass spectrometer (Hiden QGA quantitative gas analysis system, Hiden Analytical) for N_2 and O_2. Equations 5, 6, 7, and 8 have been used to calculate the NO_2 conversion (*X*) and the product selectivity (*S*). The energy efficiency, *EE*, for the dissociation of NO_2 is defined by Equation 9. Each data point is an average of 3 consecutive measurements, with an error of < ± 3% for NO_2 conversions and < ± 4% for product selectivities. The N balance is typically close to within 99% based on the concentration of NO_2, NO, N_2, and N_2O as determined by FTIR and mass spectrometry.

$$X_{NO_2} = \frac{[NO_2]_{inlet} - [NO_2]_{outlet}}{[NO_2]_{inlet}} \times 100\% \quad \text{(Equation 5)}$$

$$S_{N_2} = \frac{[NO_2]_{inlet} - [NO_2]_{outlet} - 2[N_2O]_{outlet} - [NO]_{outlet}}{[NO_2]_{inlet} - [NO_2]_{outlet}} \times 100\% \quad \text{(Equation 6)}$$

$$S_{N_2O} = \frac{[NO_2]_{inlet} - [NO_2]_{outlet} - 2[N_2]_{outlet} - [NO]_{outlet}}{[NO_2]_{inlet} - [NO_2]_{outlet}} \times 100\% \quad \text{(Equation 7)}$$

$$S_{NO} = \frac{[NO_2]_{inlet} - [NO_2]_{outlet} - 2[N_2O]_{outlet} - 2[N_2]_{outlet}}{[NO_2]_{inlet} - [NO_2]_{outlet}} \times 100\% \quad \text{(Equation 8)}$$

$$EE(\text{mmol kJ}^{-1}) = \frac{n_{NO_2}\ \text{input(mmol s}^{-1}) - n_{NO_2}\text{output(mmol s}^{-1})}{\text{Discharge power (kW)}} \quad \text{(Equation 9)}$$

Continuous wave (CW) EPR spectroscopy

EPR spectroscopy has been used to investigate the local environment of the Cu^{2+} ions and their interaction with NO_2. Spectra were recorded at X-band (~9.5 GHz) with a Bruker EMX 300 EPR spectrometer equipped with a high-Q resonator and a

liquid He cryostat. Recording of the half-field "forbidden" transitions involved an ER 4116DM dual mode resonator operating at ~9.6 GHz in perpendicular mode and at ~9.4 GHz for the parallel B_1 pattern. Theoretical modeling of the EPR spectra was performed using the EasySpin software in MATLAB (more details are given in the supplemental information)

Ex situ X-ray absorption spectroscopy

Ex situ X-ray absorption spectroscopy measurements were performed at the Cu K-edge (8,979 eV) on the B18 beamline at the Diamond Light Source (Didcot, UK). Measurements were performed in transmission mode using a quick scanning extended X-ray absorption fine structure (QEXAFS) setup with fast-scanning Si(111) double crystal monochromators for the Cu edge. The data processing was performed using IFEFFIT with the Demeter package (Athena and Artemis). The fitting parameters were $S_0^2 = 0.86$; fit range $3 < k(Å^{-2}) < 12.4$, $1 < R(Å) < 3$; number of independent points = 11.7. Each sample was preheated from room temperature to 250°C at a rate of 10°Cmin^{-1} in He to remove water and other adsorbed species, and then transferred into a sealed sample cell inside a glovebox. The metal particle size was calculated based on the previously reported method.[2]

In situ and *in operando* DRIFTS analysis

DRIFTS measurements were carried out using a Bruker Vertex 70 FTIR spectrometer equipped with a liquid N_2-cooled detector. The spectra were recorded at a 4 cm^{-1} resolution, and each spectrum was averaged 128 times. For the IR measurements of the bare samples, the sample was activated at 250°C under Ar (99.999%, BOC Gas) for 4 h to remove adsorbed water from the pores. The spectrum of KBr, thermally dried at 250°C in Ar for 4 h, was used as the background.

In situ DRIFTS measurements of the catalysts as a function of NO_2 adsorption were also conducted. The sample was first activated at 250°C under Ar for 4 h to remove adsorbed water from the pores. The sample temperature was then reduced to room temperature for all of the measurements. The spectrum of the activated sample was used as the background reference for the spectra of NO_2-loaded samples. A stream of 500 ppm NO_2 diluted in Ar with a total flow rate of 50 mL min^{-1} was introduced to the DRIFTS cell to establish the NO_2 adsorption for each sample. The gas mixture was then switched to pure Ar at a total flow rate of 50 mL min^{-1} to purge the cell and remove the gas phase NO_2 and weakly adsorbed NO_2 to reveal the strongly bound NO_x species on the catalysts.

In operando DRIFTS measurements of the dissociation of NO_2 over the catalyst under plasma were measured using a Bruker Tensor 70 FTIR spectrometer (resolution = 4 cm^{-1}) with a specifically designed *in situ* plug flow cell with the plasma generated in the catalyst bed using a modified Spectra Tech Collector II DRIFTS accessory.[17] The catalyst was activated at 120°C under He (99.999%, BOC Gas) for 4 h to remove adsorbed water. The temperature of the sample was then reduced to room temperature, and the spectrum of the desolvated sample at room temperature was used as the background reference for the following reaction. The reaction was performed at 25°C using a stream of 500 ppm NO_2 diluted in He with a total flow rate of 50 mL min^{-1}. The plasma generator was an alternating current power source (PVM500 model), and the electrical parameters were monitored using an oscilloscope (Tektronix TBS1062) that was connected to the reactor through a high-voltage probe (Tektronix, P6015). The applied voltage was 7.5 $\pm$ 0.5 kV at a frequency of 26 kHz and a SEI of ~0.2 kJ L^{-1}.

Dynamic breakthrough and temperature-programmed desorption of NO_2

Dynamic breakthroughs of NO_2 and NO_2-TPD experiments were performed to determine the NO_2 adsorption capacity and adsorbate-adsorbent strength for each catalyst. In a typical experiment, the powder sample was packed in a fixed-bed reactor equipped with a Bruker Matrix MG5 FTIR spectrometer (resolution = 0.5 cm^{-1}) as the detector. The sample was first activated at 250°C under a dry He flow at 100 mL min^{-1} (99.999%, BOC Gas) for 20 h. After activation, the temperature of the reactor was decreased to 25°C and a gas mixture of 500 ppm NO_2 diluted in He was introduced to the fixed bed to establish the adsorption of NO_2. The complete breakthrough of NO_2 is observed when the concentration of NO_2 at the outlet is equal to that of the inlet. On saturation, the gas stream was switched to pure He (flow rate = 100 mL min^{-1}) to remove the physical (weakly) adsorbed NO_2 from the sample until a stabilized IR spectrum is obtained. The temperature of the reactor was then increased at a rate of 5°C min^{-1} under a dry He flow to measure the desorption of strongly adsorbed NO_2. The signals for CO, CO_2, H_2O, and NO_x (N_2O, NO, and NO_2) were monitored by the FTIR spectrometer continuously until desorption was complete.

SUPPLEMENTAL INFORMATION

Supplemental Information can be found online at https://doi.org/10.1016/j.xcrp.2021.100349.

ACKNOWLEDGMENTS

We thank the EPSRC, the Royal Society, and the University of Manchester for funding and the EPSRC for funding of the National EPR Facility at Manchester. This project has received funding from the European Research Council (ERC) under the European Union's Horizon 2020 research and innovation programme (grant agreement no. 742401, *NANOCHEM*). We thank Diamond Light Source for access to the Beamlines I11 and B22. We acknowledge Diamond Light Source beamline staff and the UK catalysis Hub Block Allocation Group (BAG) Programme Mode Application, in particular Dr. Veronica Celorrio, Dr. Nitya Ramanan, Dr. June Callison, and Dr. Donato Decarolis, for the provision of beamtime at B18 (experiment SP19850) for collection of the data presented in this work and the initial discussion of the data. The UK Catalysis Hub is kindly thanked for resources and support provided via our membership of the UK Catalysis Hub Consortium and funded by EPSRC grant no. EP/K014706/2. This work was supported by the Henry Royce Institute for Advanced Materials funded through EPSRC grants EP/R00661X/1, EP/S019367/1, EP/P025021/1, and EP/P025498/1.

AUTHOR CONTRIBUTIONS

S.X., materials synthesis and characterization and catalysis tests, including the reactor design. S.X. and X.H., measurements and analysis of the breakthrough data and temperature-programmed desorption data. S.X., T.D.D., and D.-T.N., TEM characterization. S.X., Y.M., S.C., and C.H., DRIFTS experiments. A.W., measurement and analysis of XPS data. S.X. and C.C.T., collection and analysis of synchrotron X-ray diffraction data. S.X., L.L., and M.D.F., collection and analysis of synchrotron infrared data. S.X., E.K.G., and C.R.A.C., measurement and interpretation of the XAFS data. A.S., F.T., and E.J.L.M., measurement and interpretation of the EPR data. S.Y. and M.S., overall design, direction, and development of the project and preparation of the manuscript, with contributions from all of the authors.

DECLARATION OF INTERESTS

The authors declare no competing interests.

Received: June 25, 2020
Revised: November 14, 2020
Accepted: January 27, 2021
Published: February 17, 2021

REFERENCES

1. Han, X., Yang, S., and Schröder, M. (2019). Porous metal–organic frameworks as emerging sorbents for clean air. Nat. Rev. Chem. *3*, 108–118.

2. Beale, A.M., Gao, F., Lezcano-Gonzalez, I., Peden, C.H., and Szanyi, J. (2015). Recent advances in automotive catalysis for NO_x emission control by small-pore microporous materials. Chem. Soc. Rev. *44*, 7371–7405.

3. Bazin, P., Marie, O., and Daturi, M. (2007). General features of in situ and operando spectroscopic investigation in the particular case of $DeNO_x$ reactions. Stud. Surf. Sci. Catal. *171*, 97–143.

4. Gao, F., Walter, E.D., Kollar, M., Wang, Y., Szanyi, J., and Peden, C.H.F. (2014). Understanding ammonia selective catalytic reduction kinetics over Cu/SSZ-13 from motion of the Cu ions. J. Catal. *319*, 1–14.

5. Schmidt, J.E., Oord, R., Guo, W., Poplawsky, J.D., and Weckhuysen, B.M. (2017). Nanoscale tomography reveals the deactivation of automotive copper-exchanged zeolite catalysts. Nat. Commun. *8*, 1666–1673.

6. Wikstrom, L.L., and Nobe, K. (1965). Catalytic dissociation of nitrogen dioxide. Ind. Eng. Chem. Process Des. Dev. *4*, 191–195.

7. Mok, Y.S., Kim, J.H., Nam, I.S., and Ham, S.W. (2000). Removal of NO and formation of byproducts in a positive-pulsed corona discharge reactor. Ind. Eng. Chem. Res. *39*, 3938–3944.

8. Hu, X., Zhang, J., Mukhnahallipatna, S., Hamann, J., Biggs, M.J., and Agarwal, P. (2003). Transformations and destruction of nitrogen oxides—NO, NO_2 and N_2O—in a pulsed corona discharge reactor. Fuel *82*, 1675–1684.

9. Han, X., Godfrey, H.G.W., Briggs, L., Davies, A.J., Cheng, Y., Daemen, L.L., Sheveleva, A.M., Tuna, F., McInnes, E.J.L., Sun, J., et al. (2018). Reversible adsorption of nitrogen dioxide within a robust porous metal-organic framework. Nat. Mater. *17*, 691–696.

10. Gong, X., Zhao, R., Qin, J., Wang, H., and Wang, D. (2019). Ultra-efficient removal of NO in a MOFs-NTP synergistic process at ambient temperature. Chem. Eng. J. *358*, 291–298.

11. Li, J., Han, X., Zhang, X., Sheveleva, A.M., Cheng, Y., Tuna, F., McInnes, E.J.L., McCormick McPherson, L.J., Teat, S.J., Daemen, L.L., et al. (2019). Capture of nitrogen dioxide and conversion to nitric acid in a porous metal-organic framework. Nat. Chem. *11*, 1085–1090.

12. Ebrahim, A.M., Levasseur, B., and Bandosz, T.J. (2013). Interactions of NO_2 with Zr-based MOF: effects of the size of organic linkers on NO_2 adsorption at ambient conditions. Langmuir *29*, 168–174.

13. Ebrahim, A.M., and Bandosz, T.J. (2013). Ce(III) doped Zr-based MOFs as excellent NO_2 adsorbents at ambient conditions. ACS Appl. Mater. Interfaces *5*, 10565–10573.

14. DeCoste, J.B., Demasky, T.J., Katz, M.J., Farha, O.K., and Hupp, J.T. (2015). A UiO-66 analogue with uncoordinated carboxylic acids for the broad-spectrum removal of toxic chemicals. New J. Chem. *39*, 2396–2399.

15. Peterson, G.W., Mahle, J.J., DeCoste, J.B., Gordon, W.O., and Rossin, J.A. (2016). Extraordinary NO_2 removal by the metal-organic framework UiO-66-NH_2. Angew. Chem. Int. Ed. Engl. *55*, 6235–6238.

16. Jurado-Vázquez, T., Sánchez-González, E., Campos-Reales-Pineda, A.E., Islas-Jácome, A., Lima, E., González-Zamora, E., and Ibarra, I.A. (2019). MFM-300: from air pollution remediation to toxic gas detection. Polyhedron *157*, 495–504.

17. Zhu, L., Liu, X.Q., Jiang, H.L., and Sun, L.B. (2017). Metal–organic frameworks for heterogeneous basic catalysis. Chem. Rev. *117*, 8129–8176.

18. Xu, S., Chansai, S., Stere, C., Inceesungvorn, B., Goguet, A., Wangkawong, K., Taylor, S.F.R., Al-Janabi, N., Hardacre, C., Martin, P.A., and Fan, X. (2019). Sustaining metal-organic frameworks for water-gas shift catalysis by non-thermal plasma. Nat. Catal. *2*, 142–148.

19. Dhakshinamoorthy, A., and Garcia, H. (2012). Catalysis by metal nanoparticles embedded on metal-organic frameworks. Chem. Soc. Rev. *41*, 5262–5284.

20. Evans, J.D., Sumby, C.J., and Doonan, C.J. (2014). Post-synthetic metalation of metal-organic frameworks. Chem. Soc. Rev. *43*, 5933–5951.

21. Zhao, M., Yuan, K., Wang, Y., Li, G., Guo, J., Gu, L., Hu, W., Zhao, H., and Tang, Z. (2016). Metal-organic frameworks as selectivity regulators for hydrogenation reactions. Nature *539*, 76–80.

22. Wang, P., Zhao, H., Sun, H., Yu, H., Chen, S., and Quan, X. (2014). Porous metal–organic framework MIL-100(Fe) as an efficient catalyst for the selective catalytic reduction of NO_x with NH_3. RSC Advances *4*, 48912–48919.

23. Jiang, H., Wang, Q., Wang, H., Chen, Y., and Zhang, M. (2016). MOF-74 as an efficient catalyst for the low-temperature selective catalytic reduction of NO_x with NH_3. ACS Appl. Mater. Interfaces *8*, 26817–26826.

24. Jiang, H.X., Zhou, J.L., Wang, C.X., Li, Y.H., Chen, Y.F., and Zhang, M.H. (2017). Effect of cosolvent and temperature on the structures and properties of Cu-MOF-74 in low-temperature NH_3-SCR. Ind. Eng. Chem. Res. *56*, 3542–3550.

25. Yu, Q., Wang, H., Liu, T., Xiao, L., Jiang, X., and Zheng, X. (2012). High-efficiency removal of NO_x using a combined adsorption-discharge plasma catalytic process. Environ. Sci. Technol. *46*, 2337–2344.

26. Park, J.H., Ahn, J.W., Kim, K.H., and Son, Y.S. (2019). Historic and futuristic review of electron beam technology for the treatment of SO_2 and NO_x in flue gas. Chem. Eng. J. *355*, 351–366.

27. Yang, S., Sun, J., Ramirez-Cuesta, A.J., Callear, S.K., David, W.I., Anderson, D.P., Newby, R., Blake, A.J., Parker, J.E., Tang, C.C., and Schröder, M. (2012). Selectivity and direct visualization of carbon dioxide and sulfur dioxide in a decorated porous host. Nat. Chem. *4*, 887–894.

28. Tran, C.D., Makuvaza, J., Munson, E., and Bennett, B. (2017). Biocompatible copper oxide nanoparticle composites from cellulose and chitosan: facile synthesis, unique structure, and antimicrobial activity. ACS Appl. Mater. Interfaces *9*, 42503–42515.

29. Beale, A.M., and Weckhuysen, B.M. (2010). EXAFS as a tool to interrogate the size and shape of mono and bimetallic catalyst nanoparticles. Phys. Chem. Chem. Phys. *12*, 5562–5574.

30. Wei, T.S., Pan, K.L., Yu, S.J., Yan, S.Y., and Chang, M.B. (2018). Storage and reduction of NO_x by combining Sr-based perovskite catalyst with nonthermal plasma. Environ. Sci. Pollut. Res. Int. *25*, 35582–35593.

31. Wang, T., Liu, H., Zhang, X., Guo, Y., Zhang, Y., Wang, Y., and Sun, B. (2017). A plasma-assisted catalytic system for NO removal over CuCe/ZSM-5 catalysts at ambient temperature. Fuel Process. Technol. *158*, 199–205.

32. Kwak, J.H., Tonkyn, R.G., Kim, D.H., Szanyi, J., and Peden, C.H.F. (2010). Excellent activity and selectivity of Cu-SSZ-13 in the selective catalytic reduction of NO_x with NH_3. J. Catal. *275*, 187–190.

33. Olsson, L., and Fridell, E. (2002). The Influence of Pt oxide formation and Pt dispersion on the reactions $NO_2 \leftrightarrow NO+1/2\ O_2$ over Pt/Al_2O_3 and $Pt/BaO/Al_2O_3$. J. Catal. *210*, 340–353.

34. Abdel-Mageed, A.M., Rungtaweevoranit, B., Parlinska-Wojtan, M., Pei, X., Yaghi, O.M., and Behm, R.J. (2019). Highly active and stable single-atom Cu catalysts supported by a

metal–organic framework. J. Am. Chem. Soc. *141*, 5201–5210.

35. Lamberti, C., Bordiga, S., Salvalaggio, M., Spoto, G., Zecchina, A., Geobaldo, F., Vlaic, G., and Bellatreccia, M. (1997). XAFS, IR, and UV–Vis Study of the Cu(I) Environment in Cu(I)-ZSM-5. J. Phys. Chem. B *101*, 344–360.

36. Zuzaniuk, V.,C., Meunier, F., and Ross, J.R.H. (1999). Possible intermediates in the selective catalytic reduction of NO: differences in the reactivity of nitro-compounds and tert-butyl nitrite over γ-Al_2O_3. Chem. Commun. (Camb.), 815–816.

37. Bordiga, S., Lamberti, C., Turnes Palomino, G., Geobaldo, F., Arduino, D., and Zecchina, A. (1999). Nitrosylic complexes in Ag(I)–ZSM-5: a comparison with Cu(I)–ZSM-5. Microporous Mesoporous Mater. *30*, 129–135.

38. Meunier, F.C., Zuzaniuk, V., Breen, J.P., Olsson, M., and Ross, J.R.H. (2000). Mechanistic differences in the selective reduction of NO by propene over cobalt- and silver-promoted alumina catalysts: kinetic and in situ DRIFTS study. Catal. Today *59*, 287–304.

39. Lamberti, C., Zecchina, A., Groppo, E., and Bordiga, S. (2010). Probing the surfaces of heterogeneous catalysts by in situ IR spectroscopy. Chem. Soc. Rev. *39*, 4951–5001.

40. López-Suárez, F.E., Illán-Gómez, M.J., Bueno-López, A., and Anderson, J.A. (2011). NOx storage and reduction on a SrTiCuO3 perovskite catalyst studied by operando DRIFTS. Appl. Catal., B. *104*, 261–267.

41. Rogge, S.M.J., Bavykina, A., Hajek, J., Garcia, H., Olivos-Suarez, A.I., Sepúlveda-Escribano, A., Vimont, A., Clet, G., Bazin, P., Kapteijn, F., et al. (2017). Metal-organic and covalent organic frameworks as single-site catalysts. Chem. Soc. Rev. *46*, 3134–3184.

42. Bauer, G., Ongari, D., Tiana, D., Gäumann, P., Rohrbach, T., Pareras, G., Tarik, M., Smit, B., and Ranocchiari, M. (2020). Metal-organic frameworks as kinetic modulators for branched selectivity in hydroformylation. Nat. Commun. *11*, 1059.

43. Roessler, M.M., and Salvadori, E. (2018). Principles and applications of EPR spectroscopy in the chemical sciences. Chem. Soc. Rev. *47*, 2534–2553.

44. Uiterkamp, A.J.M.S. (1972). Monomer and magnetic dipole-coupled $Cu^{(2+)}$ EPR signals in nitrosylhemocyanin. FEBS Lett. *20*, 93–96.

45. Uiterkamp, A.J.M.S., and Mason, H.S. (1973). Magnetic dipole-dipole coupled Cu(II) pairs in nitric oxide-treated tyrosinase: a structural relationship between the active sites of tyrosinase and hemocyanin. Proc. Natl. Acad. Sci. USA *70*, 993–996.

46. Xu, S., Whitehead, J.C., and Martin, P.A. (2017). CO_2 conversion in a non-thermal, barium titanate packed bed plasma reactor: the effect of dilution by Ar and N_2. Chem. Eng. J. *327*, 764–773.

47. Xu, S., Khalaf, P.I., Philip, A.M., and Whitehead, J.C. (2018). CO_2 dissociation in a packed-bed plasma reactor: effects of operating conditions. Plasma Sources Sci. Technol. *27*, 075009.